Simulation of Boundary Value Problems for the Boltzmann Equation

Jens Struckmeier
Department of Mathematics
University of Kaiserslautern
P.O Box 3049
67653 Kaiserslautern
Germany

Abstract

The paper presents numerical results on the simulation of boundary value problems for the Boltzmann equation in one and two dimensions. In the one–dimensional case, we use prescribed fluxes at the left and diffusive conditions on the right end of a slab to study the resulting steady state solution. Moreover, we compute the numerical density function in velocity space and compare the result with the Chapman–Enskog distribution obtained in the limit for continuous media. The aim of the two–dimensional simulations is to investigate the possibility of a symmetry break in the numerical solution.

1 Introduction

In the following we present the numerical part of a study on boundary value problems for the Boltzmann equation; the theoretical investigation, which deals with existence results for various types of boundary conditions, is the content of Ref. [7]. The question whether the existing solutions are unique or not is still an open problem, even for one–dimensional slab geometry. One aim of the numerical simulation is to investigate two–dimensional problems with spatial symmetry, and to look for any kind of symmetry break in the numerical solution, which would indicate instability and nonuniqueness. The results computed for one–dimensional slab geometry will explain how solutions with completely diffusive boundary conditions are obtained using prescribed (Maxwellian) fluxes at one end of the slab. Here, we directly follow the theoretical investigation given in [7]. Because of the high resolution of the simulation results, we are able to compute the numerical density in the velocity space and compare the result with the Chapman–Enskog distribution obtained by considering the limit for continuous media.

In Section 2 we formulate boundary value problems for the Boltzmann equation and discuss different kinds of boundary conditions. Section 3 deals with a particle method for the numerical treatment of the Boltzmann equation. A detailed description can be found in Ref. [8] and we only present the basic ideas of the scheme. The main part of the paper is given in Section 4, where we present various numerical results for one– and two–dimensional boundary value problems.

2 Boundary Value Problems for the Boltzmann Equation

We are concerned with the steady Boltzmann equation given in the form

$$v \cdot \nabla_x f = Q(f), \quad x \in \Omega, \quad v \in I\!R^3 \tag{2.1}$$

on the one– or two–dimensional domain $\Omega \subset I\!R^n$, $n = 1, 2$ and various boundary conditions at $\partial\Omega$. The right hand side of (2.1) is the collision operator, describing binary collisions between gas particles, and is given in the form

$$Q(f) = Q^+(f) - L(f)f$$

and

$$Q_+(f) = \int_{I\!R^3}\int_{S_+} B(|v - v_*|, n) f(v') f(v'_*) \mathrm{d}n\mathrm{d}v_*, \tag{2.2}$$

$$L(f) = \int_{I\!R^3}\int_{S_+} B(|v - v_*|, n) f(v_*) \mathrm{d}n\mathrm{d}v_* \,. \tag{2.3}$$

Here, S_+ is the hemisphere corresponding to $(v - v_*, n) > 0$ and the pair (v', v'_*) is given by the collision transformation

$$J : (v, n, v_*) \to (v', -n, v'_*)$$

with

$$\begin{aligned} v' &= v - n(v - v_*, n), \\ v'_* &= v_* + n(v - v_*, n) \,. \end{aligned}$$

A typical form for the collision kernel B is

$$B(|v - v_*|, n) = |v - v_*|^k h(\theta) \,,$$

where θ is the polar angle of n relative to a polar axis in direction $v - v_*$, e.g., $k = 1$ yields the hard–sphere gas.

Equation (2.1) is complemented with some appropiate boundary conditions at $\partial\Omega$. A typical form of boundary conditions is to prescribe the ingoing distribution function, as used for example in Ref. [1], where the authors proved the existence of a measure–valued solution for the one–dimensional slab geometry. A second class – also known as gas–surface interaction laws [4] – are reflective boundary conditions, where the ingoing flux is defined in terms of the outgoing flux modified according to a given boundary kernel. This type of boundary condition is necessary, if one wants to predict, e.g., the aerothermodynamic behaviour of a re–entry vehicle under rarefied gas conditions.

The general type of (reflective) boundary conditions is given by

$$|v \cdot n(x)| f(t, x, v) = \int_{v' \cdot n(x) < 0} |v' \cdot n(x)| R(t, x; v' \to v) f(t, x, v') \mathrm{d}v' \tag{2.4}$$

for $v \cdot n(x) > 0$, where $n(x)$ is the inner normal at $x \in \partial\Omega$. The boundary kernel R should satisfy the conditions

$$R(t, x; v' \to v) \geq 0, \tag{2.5}$$

$$\int\limits_{v\cdot n(x)>0} R(t,x;v'\to v)\mathrm{d}v = 1 \tag{2.6}$$

Especially, Equation (2.6) guarantees mass conservation at the boundary $\partial\Omega$. Examples for R satisfying (2.5), (2.6) are specular reflection, i.e.

$$R(v'\to v,x) = \delta\left(v'-v+2n(n\cdot v)\right)\ , \tag{2.7}$$

diffusive kernels

$$R(v'\to v,x) = \frac{2\beta(x)^2}{\pi}|v\cdot n(x)|\mathrm{e}^{-\beta(x)v^2}\ , \tag{2.8}$$

where $\beta(x)$ is a given (inverse) temperature profile along $\partial\Omega$, the Maxwell model, which is given as a linear combination of (2.7) and (2.8), and the Cercignani–Lampis model which includes two accomodation coefficients [4]. Due to the lack of information on appropiate accomodation coefficents, the diffusive kernels (2.8) are the most widely used (reflective) boundary conditions in real applications.

3 Particle Schemes for the Boltzmann Equation

The particle method used to compute the solution of boundary value problems is the so–called Finite–Pointset–Method (FPM) as described in Ref. [8]. We shortly recall the basic ideas behind this numerical scheme.

We consider the instationary Boltzmann equation in the form

$$f_t + v\cdot\nabla_x f = Q(f) \tag{3.1}$$

together with an appropiate initial condition at $t=0$ and boundary conditions like the one discussed in the previous section. The solution $f(t,x,v)$ of (3.1) is interpreted as the density of the corresponding time–dependent measure denoted by $\mu_t(x,v)$ and μ_t is approximated by a discrete measure of the form

$$\delta_{\omega_n(t)} = \sum_{i=1,\dots,n}\alpha_i\delta_{p_i(t)}\,, \tag{3.2}$$

generated by a so–called finite pointset $\omega_n(t) = \{(p_i(t),\alpha_i)\}_{i=1,\dots,n}$. Here, $p_i = (x_i,v_i)$ denotes the position resp. velocity of a particle and α_i the corresponding weight, which may also be a function of t. In the following we assume that the weights are independent of t.

For a fixed time $t\geq 0$ a sequence $\{\delta_{\omega_n(t)}\}_{n\in\mathbb{N}}$ should form a convergent approximation in the sense of weak-$*$ convergence of measures denoted in the following by $\delta_{\omega_n}(t)\xrightarrow{w^*}\mu_t$, i.e.

$$\int\limits_{\Omega\times\mathbb{R}^3}\Phi(x,v)\mathrm{d}\delta_{\omega_n(t)}\xrightarrow{n\to\infty}\int\limits_{\Omega\times\mathbb{R}^3}\Phi(x,v)\mathrm{d}\mu_t\,, \tag{3.3}$$

where (3.3) should hold for all bounded and continuous functions Φ on $\Omega\times\mathbb{R}^3$.

The dynamic behaviour of the particles defined by the discrete measure in (3.2) is derived using a splitting method over a small time intervall $[t,t+\Delta]$ to separate the left hand side of (3.1) from the collision operator, yielding the two equations

$$f_t + v\cdot\nabla_x f = 0\,, \tag{3.4}$$

which describes the free flow of particles and

$$f_t = Q(f)\,, \tag{3.5}$$

which describes the collision between particles.

Equation (3.4) is solved over a small time increment $[t, t+\Delta]$ simply by moving each x-coordinate in (3.2) to the new position $x_i + \Delta t v_i$, i.e.

$$\sum_{i=1,\dots,n} \alpha_i \delta_{(x_i(t),v_i(t))} \quad \stackrel{3.4}{\longrightarrow} \quad \sum_{i=1,\dots,n} \alpha_i \delta_{(x_i(t)+\Delta t v_i(t),v_i(t))}\,.$$

If the trajectory $\{x_i(t) + \tau v_i(t) \,:\, \tau \in [0,\Delta t]\}$ hits the boundary of spatial domain, one has to incorporate the corresponding boundary condition.

The numerical simulation of equation (3.5) is much more complicated. Introducing a explicit discretization in (3.5) yields (for t = 0)

$$f(\Delta t, x, v) = f(0, x, v) + \Delta t Q(f)(0, x, v)\,. \tag{3.6}$$

The main difficulty in equation (3.6) is, that Q is a local operator in space and one has to introduce a mollifier with respect to $x \in \Omega$. Hence, instead of the discrete measure given by (3.2), we use a discrete measure in the form

$$\delta_{\hat{\omega}_n(t)} = \sum_{i=1,\dots,n} \alpha_i \beta^{\Delta x}(x, x_i(t)) \delta_{v_i(t)}\,,$$

to approximate the solution of (3.6), where $\beta^{\Delta x}(x, x_i(t))$ denotes some spatial mollifier for the point measure located at $x_i(t)$. The standard way of doing this is to use a subdivision of the spatial domain into small cells c_i, such that $\bigcup_{i=1,\dots,m} c_i = \Omega$, and to use the mollifier

$$\beta^{\Delta x}_{\mathrm{hom}}(x, y) = \sum_{i=1,\dots,m} \frac{\mathcal{X}_{c_i}(x)\mathcal{X}_{c_i}(y)}{\mathrm{vol}(c_i)}\,, \tag{3.7}$$

which corresponds to the assumption that the density function $f(t, x, v)$ is spatially homogeneous in each cell c_i. The advantage of using (3.7) is that Equation (3.6) reduces to a system of homogeneous Boltzmann equations, i.e. one has to solve in each cell c_i the (time–discretized) spatially homogeneous Boltzmann equation, which will be discussed in the following.

Because we want to approximate the solution by a discrete measure, it is convenient to switch to the measure formulation of the problem, i.e. we consider the x–independent measure equation

$$\mu_{\Delta t} = \mu_0 + \Delta t Q(\mu_0) \tag{3.8}$$

Now, using the decomposition of the collision operator Q into the gain and loss term, i.e. $Q(\mu_0) = Q^+(\mu_0) - \mu_0 L(\mu_0)$, yields

$$\mu_{\Delta t} = (1 - \Delta t L(\mu_0))\,\mu_0 + \Delta t Q^+(\mu_0) \tag{3.9}$$

With the collision transformation J, Equations (2.2), (2.3) and assuming that $\|\mu_0\|_1 = 1$, Equation (3.9) reads

$$\int_{R^3} \Phi(v) \mathrm{d}\mu_{\Delta t} = \int_{R^3} \{\Delta t B(|v - v_*|, n)\Phi(v') + (1 - \Delta t B(|v - v_*|, n))\Phi(v)\}\,\mathrm{d}n\mathrm{d}\mu_0\mathrm{d}\mu_0\,,$$

which should hold for all $\Phi \in \mathcal{C}_b(\mathbb{R}^3)$. Introducing $s \in [0,1]$ and the transformation T defined by

$$T(v, v_*, \eta, s) = \begin{cases} v' & s \leq \Delta t B(|v - v_*|, n) \\ v & \text{else} \end{cases} , \tag{3.10}$$

we finally obtain the form

$$\mu_{\Delta t} = (\mu_0 \times \mu_0 \times \omega \times \lambda) \circ T^{-1} . \tag{3.11}$$

Here, $\omega(\eta)$ denotes the measure of the collision parameter and $\lambda(s)$ the uniform measure on the intervall $[0,1]$.

The crucial part in (3.11) is the generation of the product $\mu_0 \times \mu_0$: the measure μ_0 is just known in the form of a discrete approximation by $\delta_{\omega_n} \xrightarrow{w^*} \mu_0$. whereas the two measures ω and λ are given and continuous. On the other hand, if $\{\delta_{\kappa_n}\}_{n \in \mathbb{N}}$ is a sequence which converges weak–$*$ to $\mu_0 \times \mu_0 \times \omega \times \lambda$, then, applying the transformation T, yields a weak–$*$ convergent sequence for the unknown measure $\mu_{\Delta t}$, because T is a.e. continuous.

It is beyond the scope of the paper to discuss the existing algorithms, how to calculate approximations of the product measure $\mu_0 \times \mu_0$, if μ_0 is given only as an approximation by discrete measures. We refer the reader to Refs. [4] and [8].

Due to the explicit time discretization in (3.6), the size of the time step Δt has to be small enough to ensure positivity of the function $f(\Delta t, x, v)$ and, moreover, the collision kernel has to be truncated. E.g., for a hard–sphere gas, the kernel is proportional to $|v - v_*|$ and therefore obviously unbounded. Particle schemes, which use an implicit discretization, can be found in Refs. [2] and [11]. Using partial explicit/implicit discretization techniques, it is futhermore possible to construct even second order discretization schemes [12].

Recently it was shown how to derive particle schemes directly for the stationary equation (with Maxwellian molecules) [2], [3]. The scheme is quite similar to the one presented above, except, that each particle is equipped with an own time step for the free flow and that all particles undergo a collision in each time step.

4 Numerical Results

In the following two subsections we present some typical results obtained by a numerical simulation method for boundary value problems of the Boltzmann equation. Subsection 4.1 deals with one–dimensional slab geometry as discussed in [1] and recently in [7]. Some results for two–dimensional geometry are given in Subsection 4.2.

4.1 One–Dimensional Slab Geometry

We consider the (time–dependent) Boltzmann equation on the slab $0 \leq x \leq 1$,

$$\frac{\partial f}{\partial t} + \xi \frac{\partial f}{\partial x} = Q(f) , \tag{4.1}$$

with boundary conditions

$$f(t, 0, v) = j^- m_0(v), \quad \xi > 0 \tag{4.2}$$

$$f(t, 1, v) = - \int\limits_{\xi' > 0} \frac{\xi'}{\xi} R(v' \to v) f(t, 1, v) \mathrm{d}v, \quad \xi < 0 \tag{4.3}$$

for all $t > 0$. Here, j^- is some positive constant and $m_0(v)$ a normalized Maxwellian,

$$m_0(v) = \frac{2\beta_0^2}{\pi} \mathrm{e}^{-\beta_0 v^2} .$$

Equation (4.1) is completed by the initial condition $f(0,x,v) = \overset{o}{f}(x,v)$. In [7] the boundary conditions (4.2),(4.3) were used to prove the existence of a measure–valued solution for the corresponding steady state problem with purely diffusive boundary conditions. The simulation of the time–dependent problem (4.1) is expected to produce a stationary solution which satisfies in addition the condition

$$\lim_{t\to\infty} \int\limits_{\xi<0} |\xi| f(t,0,v)\mathrm{d}v = \int\limits_{\xi>0} \xi j^- m_0(v)\mathrm{d}v = j^- \tag{4.4}$$

Relation (4.4) follows from mass conservation (see (2.6)) and the one–dimensional geometry: integrating the (steady) Boltzmann equation with respect to v yields

$$\frac{\mathrm{d}j}{\mathrm{d}x} = 0 \tag{4.5}$$

for the mass flux $j(x) = \int v f(x,v)\mathrm{d}v$. Because of (2.6) and (4.3), it follows that $j(1) = 0$ and $j(x) = 0$ for all $0 \le x \le 1$. Hence, for every solution $f = f(x,v)$ of the time–independent version of (4.1) with boundary conditions (4.2), (4.3) it holds that

$$\int\limits_{\xi<0} |\xi| f(0,v)\mathrm{d}v = j^-$$

For the following numerical result we use a diffusive boundary condition at $x = 1$, i.e. $R(v' \to v) = \xi m_1(v)$, $\xi < 0$ where

$$m_1(v) = \frac{2\beta_1^2}{\pi} \mathrm{e}^{-\beta_1 v^2} \tag{4.6}$$

To simulate the instationary problem (4.1) the interval $[0,1]$ is divided into M subintervals $c_i = [\frac{i-1}{M}, \frac{i}{M})$ of length $\Delta x = 1/M$ and the density $f(t,x,v)$ is assumed to be spatially homogeneous in each cell, i.e. we use the mollifier $\beta(x,y) = M \sum \mathcal{X}_{c_i}(x)\mathcal{X}_{c_i}(y)$ (see Section 2).

The collision process is reduced to a set of homogeneous Boltzmann equations based on the given cells c_i. Generalized Halton–sequences [10] are used to generate the pointsets, which approximate the initial condition as well as the boundary condition at $x = 0$.

Boundary condition (4.3) is incorporated into the free movement of the particles: if a particle hits the right boundary of the slab, it is reflected according to the given Maxwellian distribution given by (4.6).

The boundary condition (4.2) is realized by simulating an additional cell c_0 of size δx at the left side of the slab geometry. In every time step c_0 is filled with a particle ensemble according to the mass flux j^- and a Maxwellian distribution with temperature β_0. During the free movement some particles will enter the slab geometry at $x = 0$. All other particles are deleted at the end of a time step.

The interval is divided into 20 subintervalls (cells). In each cell $N_0 = 1000$ particles are used to approximate the initial condition. The mean free path λ is equal to 0.1 which results in a Knudsen number of 0.1. The temperature at $x = 1$ is fixed at a value of 2. The time step Δt is chosen such that $<\overset{o}{v}> / \Delta t = 1$, where $<\overset{o}{v}>$ denotes the averaged velocity in positive x–direction of the

Maxwellian initial condition at temperature 1. The temperature of the Maxwellian $m_0(v)$ is equal to 0.1. Moreover, we use 20 independent samples to reduce the fluctuations in the instationary numerical results and 200 time steps in each sample to average the values in the stationary state.

The ingoing mass flux j^-, which enters the problem as a free parameter, is realized using lN_0, $l \in \mathbb{R}_+$, particles to approximate the Maxwellian distribution in the artificial boundary cell c_0.

Figure 1 shows the instationary behaviour of the (normalized) total particle number $\frac{N_{tot}(t)}{MN_0}$ for different values of l. After about 500 time steps this quantity reaches a stationary state, which means that the outgoing mass flux at $x = 0$ balances the ingoing mass flux.

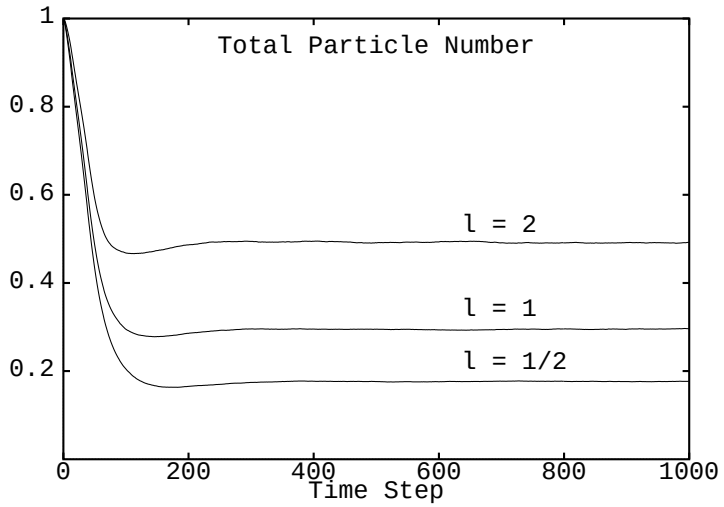

Fig. 1. Instationary Total Particle Number.

This effect is shown in Fig. 2 where the in– and outgoing mass flux is plotted versus the first 500 time steps. The quantities shown are the corresponding amount of particles which leave and enter the slab at $x = 0$ (normalized by N_0). The (time–independent) horizontal curves are the ingoing fluxes (upper line for $l = 2$, lower line for $l = 1/2$), the two time–dependent curves in Fig. 2 are the outgoing fluxes for $l = 2$ (upper curve) and $l = 1/2$ (lower curve).

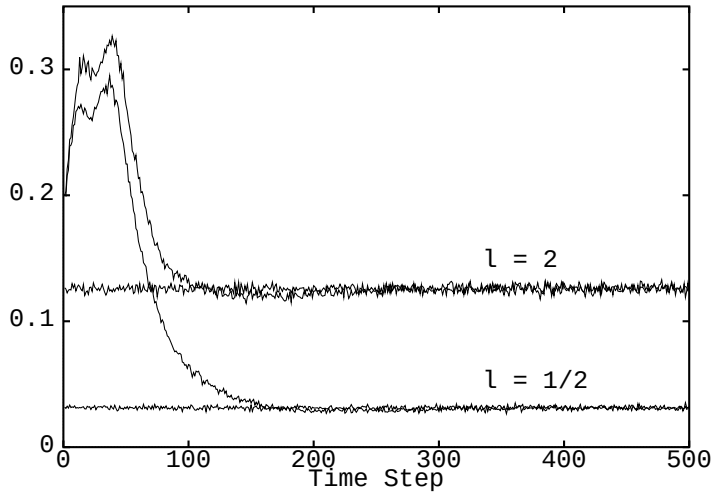

Fig. 2. In– and Outgoing Mass Flux.

The local minima which appear after about 25 time steps seem to be no artificial effect. A simulation with a larger number of particles produces the same result (see Fig. 3 with $N_0 = 4000$).

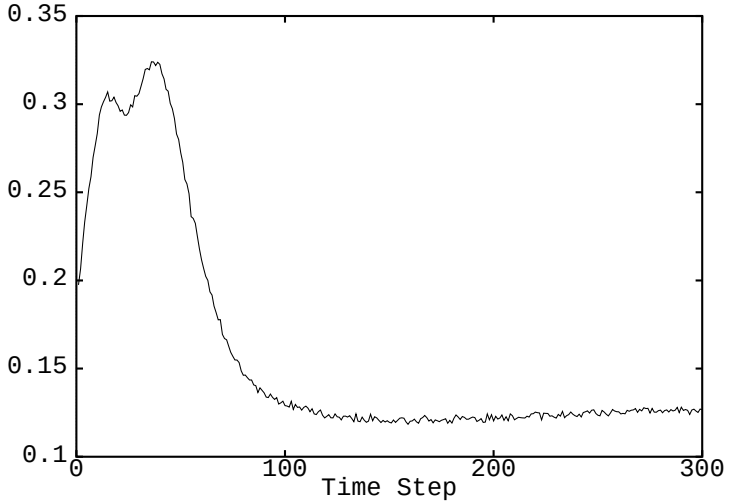

Fig. 3. Outgoing Mass Flux ($l = 2$) **with** $N_0 = 4000$**.**

This effect even increases with decreasing Knudsen number. Figure 4 shows the in– and outgoing mass flux at a Knudsen number of 0.05 (and $M = 40$).

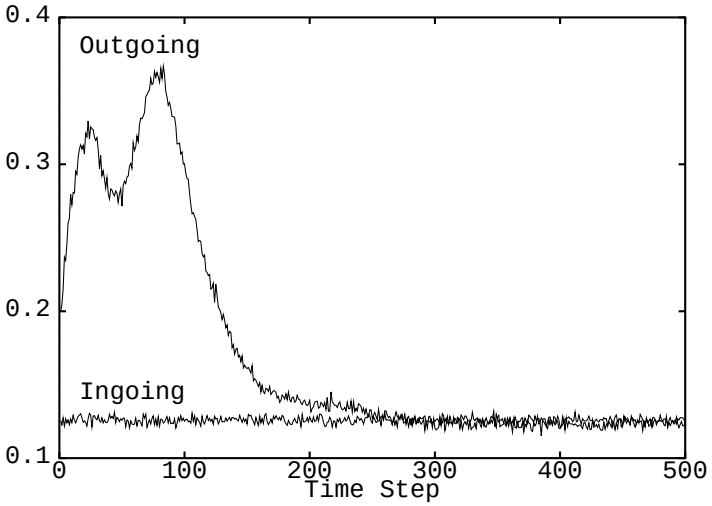

Fig. 4. In– and Outgoing Mass Flux ($l = 2$)**.**

Typical density and temperature profiles in the stationary state are plotted in Fig. 5.

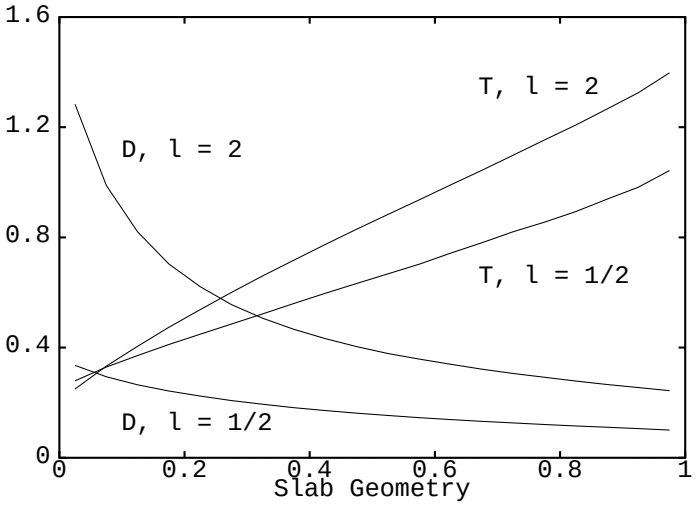

Fig. 5. Density (D) and Temperature (T) Profiles.

The various profiles are in agreement with the behaviour of the total particle number as shown in Fig. 1. The steady state value decreases with decreasing l, i.e. the gas becomes more rarefied. On the other hand, if the gas becomes more rarefied the slope of the temperature curves should decrease. For the density curves it is obvious that the maximal value is reached at $x = 0$ because $\beta_1 \ll \beta_0$ and the maximal density increases with increasing l.

Moreover, the stationary profiles shown in Fig. 4 are identical with the standard heat transfer profiles between two parallel plates at different temperatures taking a Knudsen number of 0.1ζ with

$$\zeta = \lim_{t \to \infty} \frac{M N_{in}}{N_{tot}(t)}.$$

The high resolution of the simulation results allows the calculation of the (numerical) density function in the velocity space. Figure 6 shows the distribution of each velocity component for a spatial cell close to the mid point of the slab geometry ($\lambda = 0.1$ and $l = 2$). Here, the density function is scaled, such that the macroscopic density is equal to one.

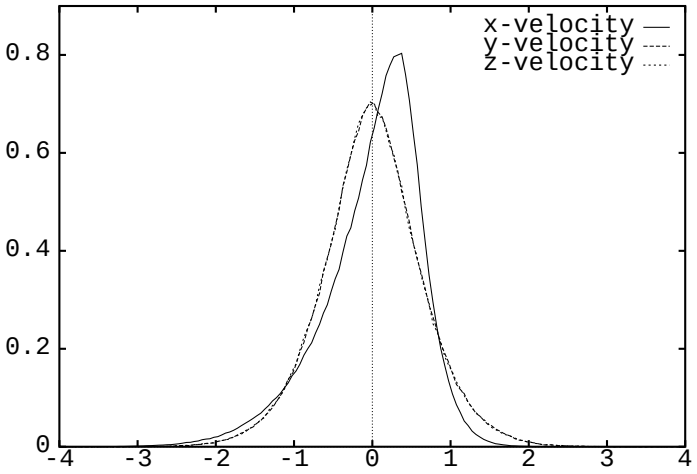

Fig. 6. Numerical Density Functions ($\lambda = 0.1$).

The distribution of the x–velocities represents a strong nonequilibrium: the maximal value is shifted to the right, because the temperature of the ingoing flux at $x = 0$ is much less than the temperature for the diffusive boundary condition at $x = 1$ and, due to the rarefied condition, the number of collisions is not large enough to produce a distribution close to a local equilibrium. Because of the one–dimensional geometry, the velocities in the y and z–direction are (numerically) almost identically distributed, but not in a local equilibrium (see also Fig. 9).

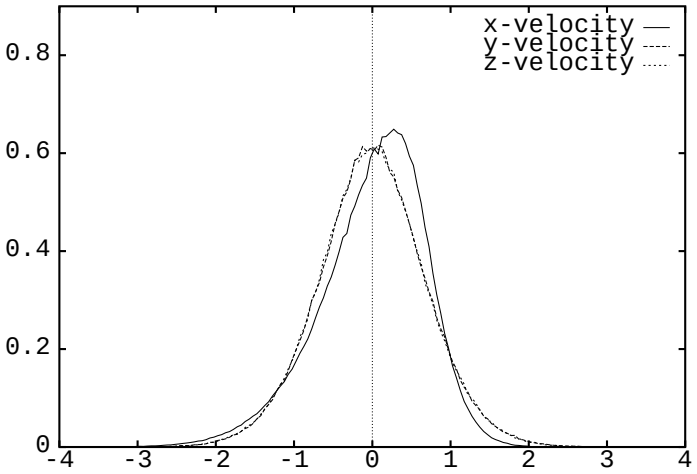

Fig. 7. Numerical Density Functions ($\lambda = 0..05$).

Decreasing the mean free path λ by a factor of 2 ($\lambda = 0.05$, $M = 40$) and 4 ($\lambda = 0.025$, $M = 80$) gives the density functions shown in Fig. 7 and 8.

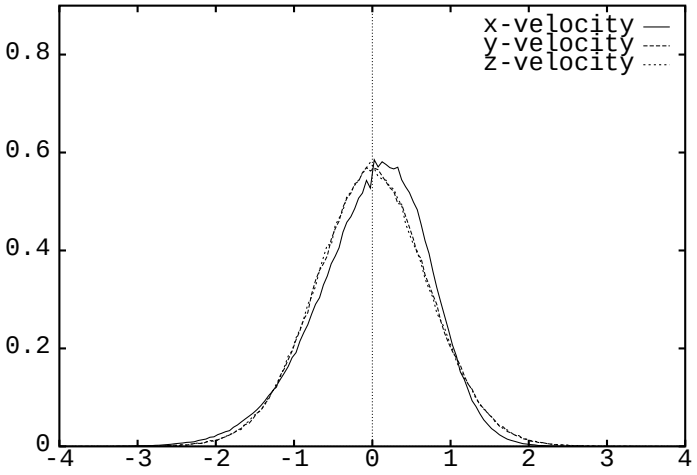

Fig. 8. Numerical Density Functions ($\lambda = 0.025$).

It is well–known, that, if $\lambda \to 0$, the one–dimensional heat transfer reaches the limit for continuous media, where the macroscopic density ρ and the temperature T satisfy the Navier–Stokes equations [5]

$$\frac{\mathrm{d}(\rho T)}{\mathrm{d}x} = 0$$
$$\frac{\mathrm{d}}{\mathrm{d}x}\left(\kappa \frac{\mathrm{d}T}{\mathrm{d}x}\right) = 0$$

Here, κ is the temperature dependent heat conduction coefficient, e.g., for a hard–sphere gas $\kappa = O(\sqrt{T})$. Moreover, the density function f can be substituted by the so–called Chapman–Enskog distribution [5]. Because the mean velocity is equal to zero and because of the one–dimensional geometry, the general form of the Chapman–Enskog distribution reduces to (assuming $\rho = T = 1$)

$$f^{\mathrm{CE}}(x, v) = \frac{1}{\pi^{3/2}} \mathrm{e}^{-|v|^2} \left(1 - \kappa \frac{\mathrm{d}T}{\mathrm{d}x} v_x \left(|v|^2 - \frac{5}{2}\right)\right) . \tag{4.7}$$

Integrating (4.7) with respect to $v_x \in \mathbb{R}$ shows, that the distribution of the y and z–velocities tend to a local Maxwellian as $\lambda \to 0$.

In Fig. 9, the solid lines shows the local Maxwellian using the numerical value of the macroscopic temperature in the corresponding cell (see Fig. 5), the points show the numerical density function for the y–velocities for $\lambda = 0.1$ (compare with Fig. 6).

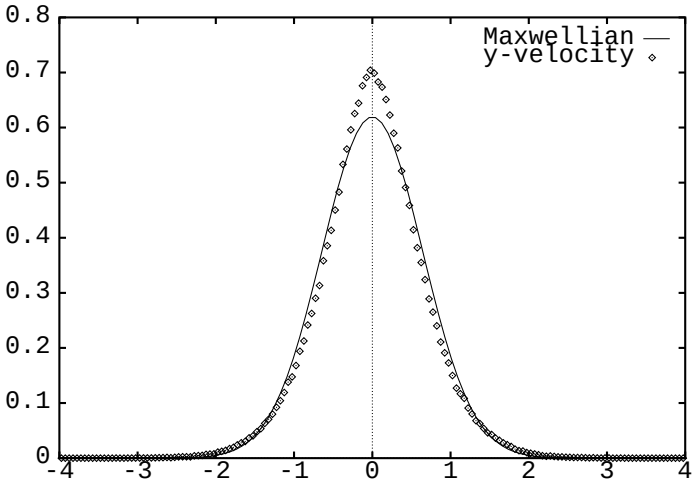

Fig. 9. Numerical Density Function ($\lambda = 0.1$) and Maxwellian.

The overshoot at $v_y = 0$ indicates, as mentioned above, that the gas ensembles is still in nonequilibrium. Decreasing the mean free path to $\lambda = 0.025$ gives a result as shown in Fig. 10.

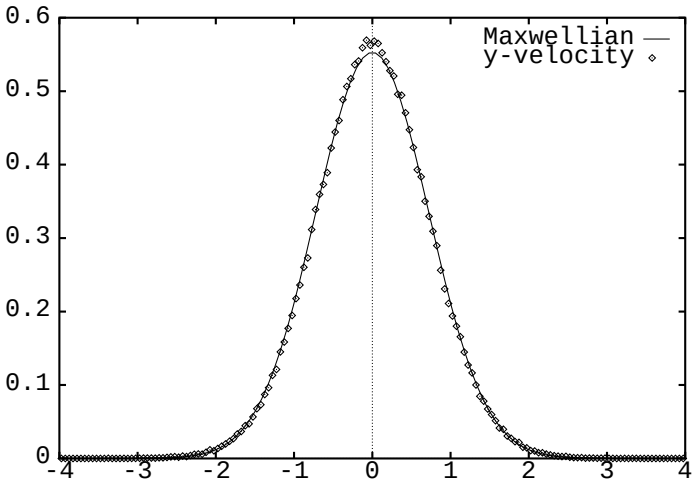

Fig. 10. Numerical Density Function ($\lambda = 0.025$) and Maxwellian.

Here, the numerical density function is already close to a local Maxwellian, indicating, that the gas ensemble is close to the continuum limit.

Remark 1
The computations were performed on a HP 9000/735 workstation at the Department of Mathematics and Statistics, University of Victoria, Canada, and required a CPU–time between 46 min for $l = \frac{1}{2}$, about 2 h for $l = 2$ (both for $\lambda = 0.1$, $M = 20$) and up to 20 h for $l = 2$, $\lambda = 0.025$ and $M = 80$.

4.2 Two–Dimensional Problems

The two–dimensional simulations are motivated by the following consideration: the existence results for boundary value problems for the Boltzmann equation on arbitrary domains do not answer the question whether the solution is unique or stable. In the case of discrete–velocity models, one can easily show, that boundary value problems may have more than one solution [6]. The idea is now to use a particle method as an experimental tool to investigate the uniqueness and stability of solutions.

Consider, for example, the one–dimensional slab geometry as presented in the previous subsection, where the y–coordinate is now included in the simulation. We consider, e.g., the spatial domain $[0,1]^2$, together with the periodic boundary conditions

$$\begin{aligned} f(x,0,v) &= f(x,1,v) \quad \text{if} \quad v_y > 0\,, \\ f(x,1,v) &= f(x,0,v) \quad \text{if} \quad v_y < 0\,. \end{aligned}$$

We compute numerical solutions of this problem and compare them with the one–dimensional profiles from the previous section, looking for symmetry breaks, bifurcations and possible nonuniqueness.

A typical two–dimensional result is shown in Fig. 11, where the boundary condition at $x = 0$ and $x = 1$ are the same as for the result given in Fig. 5 with $l = 2$. Here, we divided the unit square $[0,1]^2$ into 400 cells, i.e. 20 cells per spatial direction, which yields the same spatial resolution as for the one–dimensional simulation. The number of particles per cell is reduced from 1000 for the one–dimensional simulation down to 200 particles – due to the larger number of spatial cells – and the number of independent samples is reduced from 20 to 10, such that the CPU–times remains within a reasonable limit.

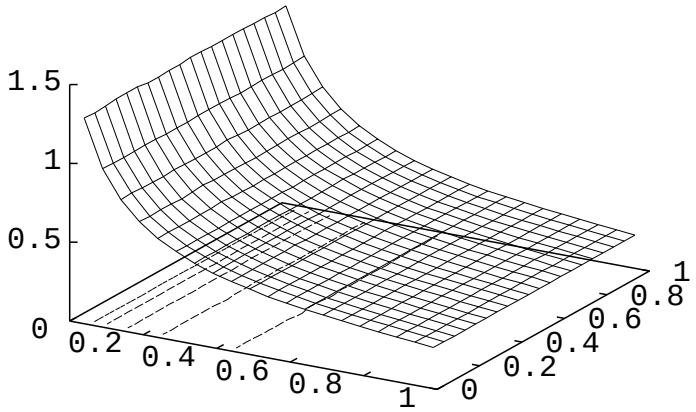

Fig. 11. Density Profile for $l = 2$.

The two–dimensional (numerical) solution is obviously independent of the space coordinate y and, moreover, for fixed y, (numerically) nearly identical with the one–dimensional solution (see Fig. 12).

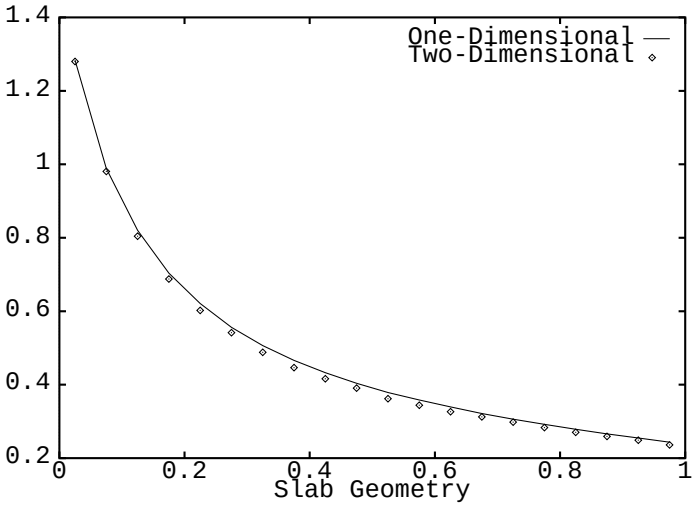

Fig. 12. One– and Two–Dimensional Density Profile.

Remark 2
The small deviation is explained by the fact that the particle number for the one–dimensional simulation is much larger than for the corresponding two–dimensional case.

A more complicated rarefied flow is investigated in the following example. Here, we use the periodic boundary conditions (4.8), (4.8) together with the diffusive conditions

$$\begin{aligned} -\xi f(0,y,v) &= j^-(y) m_{\alpha(y)}, \quad \xi < 0, \quad 0 < y < 1 \\ \xi f(1,y,v) &= j^+(y) m_{\gamma(y)}, \quad \xi > 0, \quad 0 < y < 1 \end{aligned}$$

where

$$\alpha(y) = \begin{cases} \beta_1 & \text{if } 0 \le y < \frac{1}{4} \text{ or } \frac{1}{2} \le y < \frac{3}{4} \\ \beta_0 & \text{if } \frac{1}{4} \le y < \frac{1}{2} \text{ or } \frac{3}{4} \le y \le 1 \end{cases}$$

$$\gamma(y) = \begin{cases} \beta_0 & \text{if } 0 \le y < \frac{1}{4} \text{ or } \frac{1}{2} \le y < \frac{3}{4} \\ \beta_1 & \text{if } \frac{1}{4} \le y < \frac{1}{2} \text{ or } \frac{3}{4} \le y \le 1 \end{cases},$$

$\beta_0 = 2$ and $\beta_1 = 0.1$ are two given (inverse) temperatures and $j^-(y)$ ($j^+(y)$) the y–dependent outgoing mass flux at $x = 0$ ($x = 1$).

Figure 13 shows the two–dimensional density profile obtained in the stationary state, Fig. 14 the corresponding termperature profile.

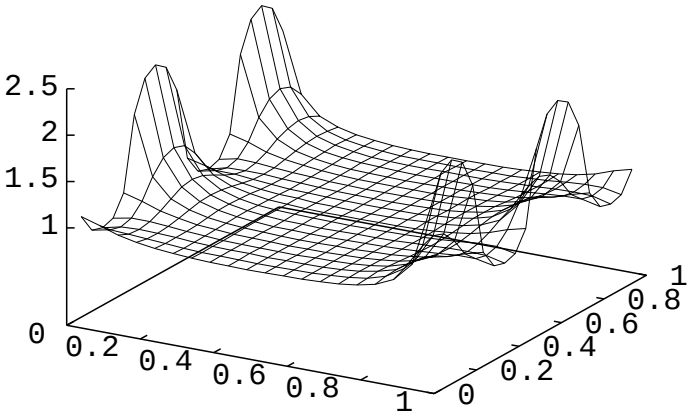

Fig. 13. Density Profile.

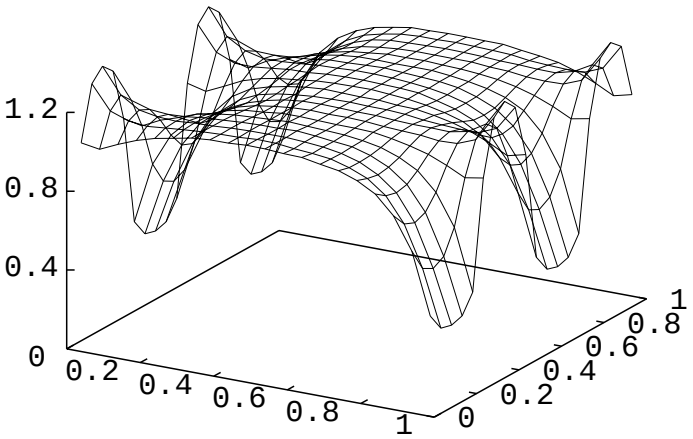

Fig. 14. Temperature Profile.

A more detailed picture on the symmetry of the solution is shown in Fig. 15 and 16, where the density and temperature profiles are given along the y–direction (for two fixed values of x).

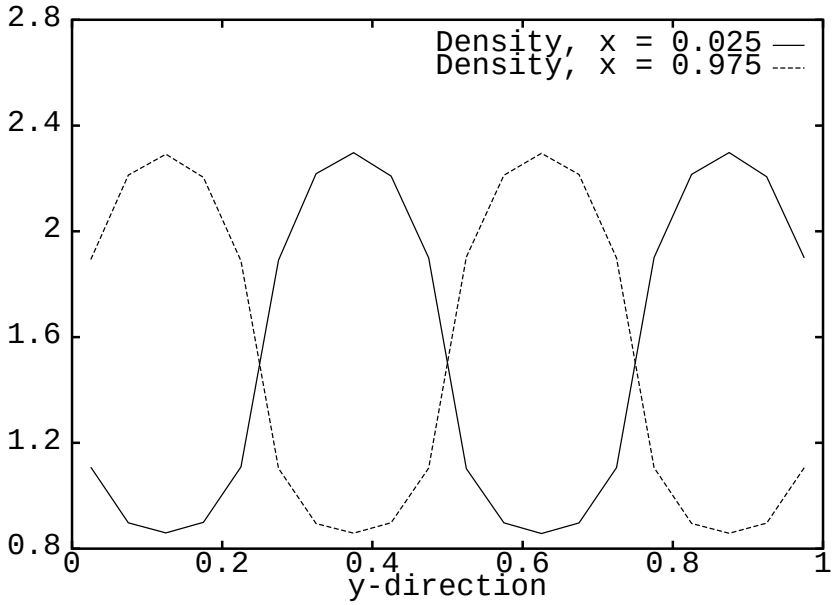

Fig. 15. Density Profiles in y–direction.

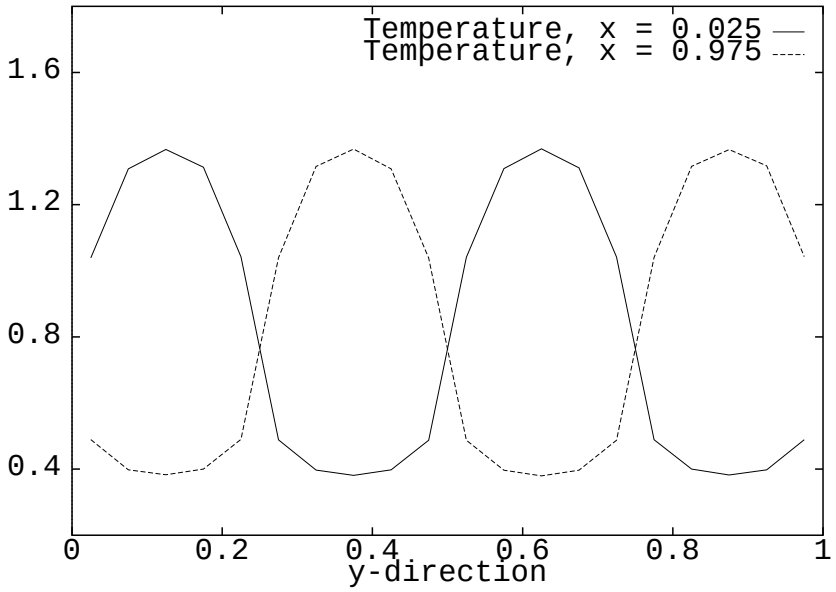

Fig. 16. Temperature Profiles in y–direction.

Remark 3
The computations were performed on a HP 9000/735 workstation at the Department of Mathematics and Statistics, University of Victoria, Canada, and required a CPU–time of 4 1/2 h for the first and 8 h for the second testcase.

Within the current investigation, a lot of different boundary conditions were implemented in the simulation. Moreover, the size of the spatial domain, which might be important in two–dimensional problem, was modified within a large range. None of the simulation results gives any indication on a symmetry break of the numerical solution. This indicates that the solutions are stable. Nevertheless, it remains a challenge to improve the existing existence and uniqueness results.

Acknowledgement: This research was supported by the Natural Sciences and Engineering Research Council of Canada under grant Nr. A 7847. The author would like to acknowledge the hospitality of the Department of Mathematics and Statistics at the University of Victoria, where this research was done.

References

[1] L. Arkeryd, C. Cercignani and R. Illner: *Measure Solutions of the Steady Boltzmann Equation in a Slab*, Commun. Math. Phys. **142**, 285–296 (1991).

[2] A.V. Bobylev and J. Struckmeier, *Implicit and Iterative Methods for the Boltzmann Equation*, preprint, to appear in Transport Theory and Statistical Physics.

[3] A.V. Bobylev and J. Struckmeier, *Numerical Simulation of the Stationary, One–Dimensional Boltzmann Equation*, preprint, to appear in Eur. J. of Mech. B/Fluids.

[4] C. Cercignani, R. Illner and M. Pulvirenti, *The Mathematical Theory of Dilute Gases*, Springer, New York (1994).

[5] F. Coron, *Derivation of Slip Boundary Conditions for the Navier–Stokes System from the Boltzmann Equation*, J. Stat. Physics, Vol. 3/4, 1989.

[6] R. Illner, *On Steady Boundary Value Problems in Discrete Kinetic Theory, and its Application to Digital Image Processing*, in: R. Monaco (ed.), Discrete Kinetic Theory, Lattice Gas Dynamics and Foundations of Hydrodynamic, World Scientific, 178–191 (1989).

[7] R. Illner and J. Struckmeier, *Boundary Value Problems for the Steady Boltzmann Equation*, preprint, submitted to Journal of Statistical Physics.

[8] H. Neunzert and J. Struckmeier, Particle Methods for the Boltzmann Equation, *ACTA NUMERICA 1995*, Cambridge University Press, Cambridge (1995).

[9] H. Niederreiter, *Random Number Generation and Quasi–Monte–Carlo Methods*, SIAM, Philadelphia (1992).

[10] J. Struckmeier, *Fast Generation of Low–Discrepancy Sequences*, preprint, to appear in J. Comp. & Appl. Math.

[11] J. Struckmeier, *Implicit Particle Methods for the Boltzmann Equation with Maxwellian Molecules*, in preparation.

[12] J. Struckmeier and K. Steiner, *Second Order Scheme for the Spatially Homogeneous Boltzmann Equation with Maxwellian Molecules*, preprint, to appear in Math. Meth. & Mod. in Appl. Sciences.